SrSi$_2$O$_2$N$_2$: Eu

- Eu^{2+}
- Eu^{3+}
- SrSiO$_3$
- heating
- amorphous film

The thermal degradation mechanism of SrSi$_2$O$_2$N$_2$:Eu^{2+} phosphor is attributed to (i) oxidation of Eu^{2+} to Eu^{3+} and (ii) the formation of the SrSiO$_3$ phase on the phosphor particle surface.

Journal of Materials Chemistry C

RSCPublishing

ARTICLE

On the thermal degradation of the green-emitting SrSi₂O₂N₂:Eu²⁺ phosphor for solid state lighting

On the thermal degradation of the green-emitting $SrSi_2O_2N_2$:Eu^{2+} phosphor for solid state lighting

Chun-Yun Wang,[a,c] Rong-Jun Xie,*[b,d] Fangzhi Li[c] and Xin Xu[a] ,

A phase pure $SrSi_2O_2N_2$:Eu^{2+} green phosphor was synthesized by the solid state reaction through the careful control of the Sr:Si ratio in the starting powder consisting of $SrCO_3$, Si_3N_4 and Eu_2O_3. The thermal degradation of the phosphor was investigated by baking it at high temperatures for 2 h. The surface states of the samples before and after baking were analyzed by SEM, HRTEM, XPS, TGA/DTA, and high temperature in-situ X-ray diffraction. The results showed that the thermal degradation became seriously when the temperature was higher than 500°C, and the degradation was caused by the formation of $SrSiO_3$ on the particle surface and the oxidation of Eu^{2+} to Eu^{3+}. It is suggested that the thermal stability can be enhanced by achieving high crystallinity as well as high phase purity of the phosphor.

1.Introduction

In recent years, solid-state lighting sources are revolutionizing an increasing number of applications due to their high efficiency, energy savings, and environmental benefits. White light-emitting diodes (wLEDs), known as the next-generation green and efficient solid-state lighting technology, are now penetrating into our daily life steadily, replacing incandescent bulbs/fluorescent tubes for general lighting, cold cathode fluorescent lamps (CCFLs) for backlighting of liquid crystal displays.[1,2] In phosphor-converted wLEDs technologies, the emission of LED chips (blue or UV light) is down-converted into useful green, yellow, or red light by phosphors. Therefore, the phosphor is one of key materials in solid state lighting, and it is required to have high quantum efficiency, suitable emission colors and emission spectra, small thermal quenching and high reliability.[2-4]

Although there are a large number of phosphors that have been discovered or developed for use in solid state lighting, a very limited number of them can be applied to white LEDs practically. Besides the problems of the emission color, quantum efficiency, spectral shape and cost, the luminescence degradation is a big challenge for those phosphors that fail to be commercialized. The luminescence degradation of a phosphor is usually caused by thermal, chemical or irradiation attacks. The degradation beyond a certain degree required by the practical applications will significantly reduce the reliability and shorten the lifetime of white LED devices, making a phosphor to loss its function as wavelength converters, even though it has high quantum efficiency and useful emission

colors.[5] For example, both alkaline earth thiogallates ($SrGaS_4$:Eu) and alkaline earth sulfides (CaS:Eu and SrS:Eu) exhibit very promising photoluminescence properties, they are seriously sensitive to moisture.[6,7] The alkaline earth orthosilicates (M_2SiO_4:Eu, M = Ca, Sr, Ba) also show very high efficiency and suitable colors, but they are easily attacked by moisture, heat and photo-irradiation.[1,3] The moisture-induced degradation can be significantly minimized by coating a water-resistant layer on the phosphor surface. The thermal degradation, however, relies closely on the crystal structure, band gap, particle quality and composition of a phosphor, which is hardly reduced by the simple surface coating.

Compared to traditional sulfide and some oxide phosphors, (oxy)nitride ones usually show high thermal/chemical stability due to their stiff structure built up on SiN_4 tetrahedral framework.[1,2,8] For instance, there are no changes in luminous efficiency of Ca-α-sialon:Eu ($Ca_{m/2}Si_{12-(m+n)}Al_{m+n}O_n N_{16-n}$, m and n represent the number of Al-N pairs and Al-O pairs substituting for Si-N pairs, respectively) and β-sialon:Eu ($Si_{6-z}Al_zO_zN_{8-z}$, z represents the number of Al-O pairs substituting for Si-N pairs) when they are exposure to 85°C/85% HR test and light irradiation for 3000 h.[9] $SrSi_2O_2N_2$:Eu^{2+} is one of important green phosphors for enhancing the color rendition and luminous efficiency of white LEDs.[10] Moreover, its color can be tuned to yellow or blue-green by substituting Ba for Sr.[11] $SrSi_2O_2N_2$ has a layered structure consisting of $SiON_3$ tetrahedra that are condensed via N atoms bridging three of the each Si atoms, while the O atoms are terminally bound to the Si atom. The Sr^{2+} ions are surrounded by six O atoms to form a

distorted trigonal prism, which is capped by a single N atom. [12] In comparison with the famous β-sialon:Eu^{2+} phosphor, $SrSi_2O_2N_2$:Eu^{2+} has higher absorption (80%) and external quantum efficiency (69%) when excited at 450 nm. [1,5,6]

The thermal stability of $SrSi_2O_2N_2$:Eu^{2+} is usually studied by in-situ measuring the thermal quenching behavior of the sample heated up to ~ 300°C and held at each temperature for several minutes. A high thermal quenching temperature of ~500°C is reported for $SrSi_2O_2N_2$:Eu. [14] But thermal quenching does not have the same meaning with thermal degradation, and thus cannot evaluate the thermal stability of a phosphor comprehensively. This is because most phosphors can have their luminescence efficiency recovered upon cooling, and no degradation but luminescence quenching is observed in this measurement. Thermal quenching is thus called an elastic deformation of luminescence intensity, whereas thermal degradation is a plastic deformation that cannot be recovered when the external attacks are removed. In this work, we attempt to evaluate the thermal degradation of $SrSi_2O_2N_2$:Eu^{2+} by recording the changes in photoluminescence intensity of the samples baked in air at high temperature. The degradation mechanism will be discussed and clarified by conducting the surface state analysis using various techniques.

2.Experimental Section

2.1 Sample preparation — The powder phosphor samples ($Sr_{1-x}Eu_xSi_2O_2N_2$) were synthesized by the conventional solid-state reaction in one step. $SrCO_3$ (Aladdin, >99.9%), α-Si_3N_4 (SN-E10, Ube Industries, Tokyo) and Eu_2O_3 (Alfa Aesar, REacton 99.999%) were used as starting materials. As the commercially available α-Si_3N_4 powder usually contains some amounts of SiO_2 as a surface layer due to partial oxidation, SiO_2 was then not further added. Appropriate amounts of starting powders with the Sr to Si ratio of 1:y (y = 1.95 - 2.20) were weighted out and mixed in an alumina mortar. 2 gram of the powder mixture was then loaded in an alumina crucible, and fired at 1500°C for 6 h under the flowing 5% N_2/H_2 atmosphere in a tube furnace. After firing, the sample was cooled down to room temperature in the furnace naturally. The powder samples were finely ground with an agate mortar for further experiments. The post-treatment of the as-prepared samples was done by annealing them at the same firing temperature for 12 h, followed by washing the powders using diluted hydrochloric acid and deionized water.

2.2 Characterizatio*n* — The phase purity of samples was analyzed by powder X-ray diffraction using Cu K_α radiation (λ = 1.54056Å) at 40 kV and 40 mA with a graphite monochromator (Bruker, D8 Advance, Germany). The photoluminescence spectra were measured at room temperature by a fluorescent spectrophotometer (F-4600, Hitachi Ltd., Japan) with a 200 W Xe-lamp under a working voltage of 700 V. The excitation and emission slits were both set at 2.5 nm, and the scanning speed was 1200 nm/min. The morphology of samples was observed with a scanning electron microscope (SEM) equipped with a black scattered electron image (FEI Quanta

FEG 250). Transmission electron microscopic (TEM) micrographs and high resolution transition electron microscopic (HR-TEM) images were obtained on a Tecnai F20 (America, FEI) electron microscope. The particle size distribution was measured with a laser diffraction analyzer (Microtrac S3500, America). Thermo gravimetric analysis (TGA) and differential thermal analysis (DTA) were conducted using a Pyris Diamond (Perkin-Elmer, America). The high temperature in situ XRD patterns were obtained by using High-Temperature Chamber Oven-Chamber : HTK 1200 N (Bruker, D8 Advance, Germany) in air up to 1100 ℃, in order to study the evolution of crystalline phases during heating. The surface elements of powders were analyzed by X-ray photoelectron spectroscopy (AXIS Ultra DLD, Shimadzu).

3. Results and discussion

3.1 Phase identification

Extensive investigations of $SrSi_2O_2N_2$:Eu^{2+} have been carried out in the literature, mainly focusing on synthesis and photoluminescence properties. [11,15-29] To the best of our knowledge, it is still a challenging problem to synthesize a phase pure $SrSi_2O_2N_2$:Eu^{2+} by the conventional solid-state reaction method. [14,30] Orthosilicates (*e.g.* Sr_2SiO_4 and $SrSiO_3$) are usually formed as impurity phases, which definitely damage the reliability of the dominant $SrSi_2O_2N_2$:Eu^{2+} phase due to their low thermal/chemical stability. Therefore, it is quite important to achieve a pure phase of $SrSi_2O_2N_2$ by carefully controlling the chemical composition and processing conditions.

In the Sr-Si-O-N system, two phases (X_1-phase and X_2-phase) were identified by Zhu. [31] X_1-phase (SrO:SiO_2:Si_3N_4 = 1:1/2:1/3) is a low-temperature phase, a single phase of which can be obtained at 1300°C. It transforms to a high-temperature X_2-phase (SrO:Si_3N_4 = 1:2/3) as temperature rises. A single X_2-phase can be achieved at 1600°C. As shown in Fig.1, the amount of Si_3N_4 in the starting powder plays a key role in controlling the phase assemblage of the fired product. A single phase of $SrSi_2O_2N_2$ is obtained when y is larger than 1.95. Below this value, $SrSiO_3$ appears as an impurity phase. The result is in good agreement with that reported by Li, *i.e.*, [15] phase pure $SrSi_2O_2N_2$ can be formed without adding SiO_2 as the starting material. The composition of y = 2 is the X_2-phase reported by Zhu. [31] An oxygen-rich phase forms when y is 2.0-2.10, and a nitrogen-rich phase produces when y is 2.10-2.20. [15]
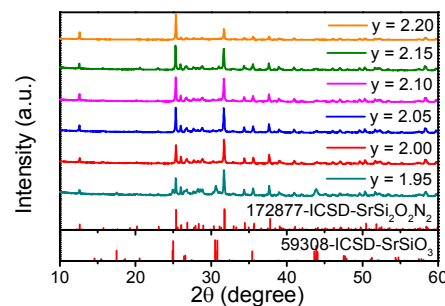

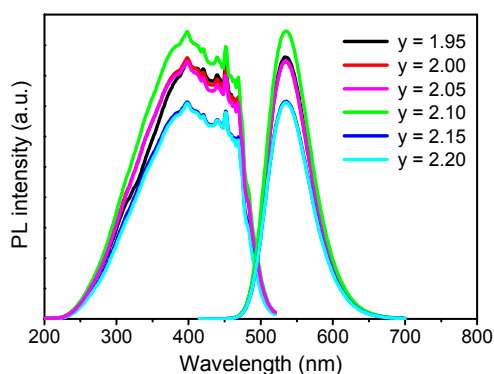**Fig. 1** XRD patterns of $SrSi_yO_2N_2$:0.05Eu^{2+} (y =1.95, 2.00, 2.05, 2.10, 2.15, 2.20) phosphor.

Fig. 2 Photoluminescence spectra of $SrSi_yO_2N_2:0.05Eu^{2+}$ (y = 1.95, 2.00, 2.05, 2.10, 2.15, 2.20) phosphor (λ_{ex} = 397 nm, λ_{em} = 534 nm).

3.2 Photoluminescence properties

Fig. 2 presents the effect of the amount of Si_3N_4 on photoluminescence spectra of the fired $SrSi_2O_2N_2:Eu^{2+}$ (5 mol%) phosphors. As seen, the photoluminescence spectra do not change in shape and position but in intensity as the Si_3N_4 content varies. The low photoluminescence intensity at y = 1.95 is ascribed to the presence of the impurity $SrSiO_3$ phase. The highest intensity is observed at y = 2.10, and this composition is used for further study.
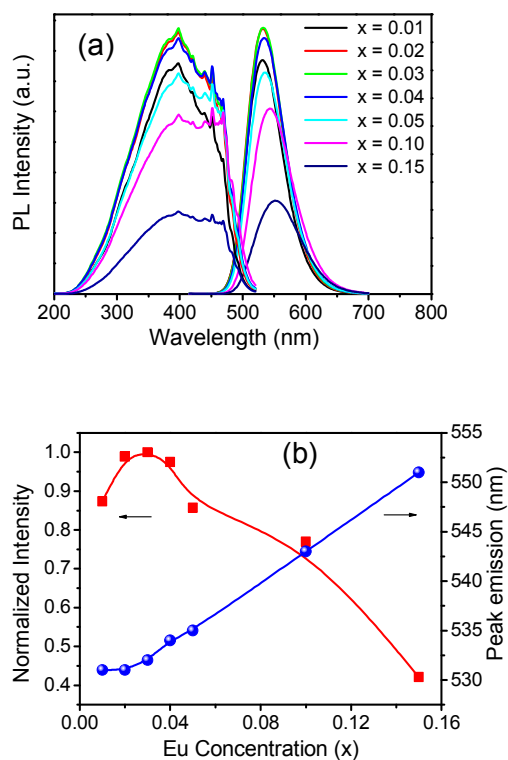

Fig. 3 (a) Photoluminescence spectra and (b) normalized emission intensity and the peak wavelength as a function of the Eu^{2+} concentration (λ_{ex} = 397 nm).

The photoluminescence properties of $SrSi_2O_2N_2:Eu^{2+}$ were investigated by varying the Eu concentration (x = 0.01 - 0.15). As shown in Fig. 3, the concentration quenching occurs at x = 0.03 where the intensity reaches its maximum. The optimal concentration is a little bit different from x = 0.04 reported by Li,[15] perhaps due to the difference in starting powders and processing conditions. The emission band is seen to red-shift by ~ 20 nm when the Eu^{2+} concentration increases. One can note that the right wing of the excitation band is enhanced as the Eu^{2+} concentration increases, implying that the 5d energy levels of Eu^{2+} are slightly lowered. Moreover, the emission band also broadens with increasing Eu^{2+} concentration. Both of these changes account for the redshift of the emission band. Correspondingly, the chromaticity coordinates shift from (0.294, 0.639) to (0.399, 0.577) for samples with x = 0.01 and 0.15.

Post-treatments of $SrSi_2O_2N_2:Eu^{2+}$ were conducted with the aim to improve the photoluminescence properties, which include prolonged annealing, powder smashing, and acid washing. These treatments play a role in reducing surface defects, removing the tiny residues, and narrowing the particle size distribution, and thus enhance the absorption of the incident light and decrease the nonradiative transition probability. [13] Fig. 4 presents the particle morphology and size distribution of $SrSi_2O_2N_2:0.03Eu^{2+}$ before and after post-treatment. One can see that the as-prepared sample (without treatment) shows large agglomerates consisting of many small particles. After the post-treatment, the particle coarsens and has a smooth surface. Furthermore, the as-prepared sample displays a bimodal particle size distribution with an average size of D_{50} = 7.35 μm, whereas the post-treated sample exhibits a very narrow particle size distribution with an average size of D_{50} = 14.86 μm. Consequently, the PL intensity is improved by 25% for the post-treated phosphor.
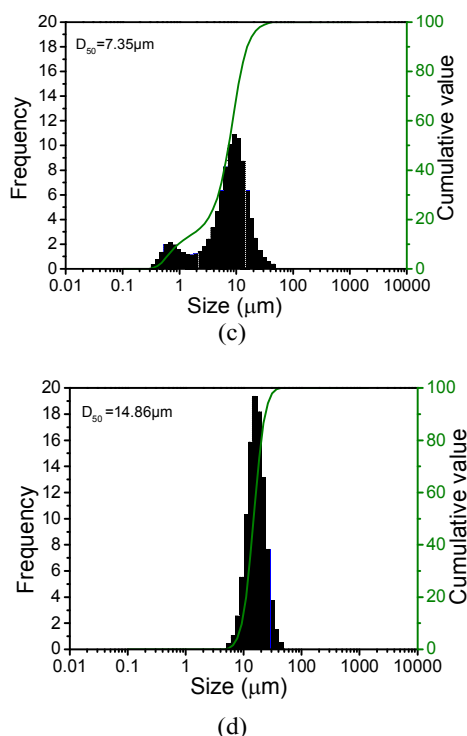

(a)

(b)

(c)

(d)
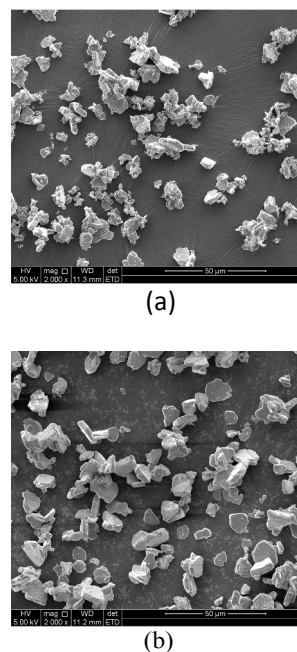
Fig. 4 SEM images of (a) as-prepared sample and (b) post-treated sample; and the particle size distribution of (c) as-prepared sample and (d) post-treated sample.

3.3 Thermal degradation under high temperature baking

Thermal stability of phosphor is considered as one of technologically important parameters, which determines the reliability of white LEDs.[13] Usually, thermal stability of a phosphor is evaluated by measuring the emission intensity and spectrum of the sample that is heated at varying temperatures for several minutes. However, the holding time at a certain temperature is too short to study the thermal stability comprehensively. In this work, we attempt to investigate the thermal stability of $SrSi_2O_2N_2:Eu^{2+}$ by recording the photoluminescence spectrum of the phosphor samples baked in air for 2 h at temperatures up to 600°C. This will help us understand both the oxidation resistance and the thermal degradation mechanism of the phosphor investigated.

As shown in Fig.5, the luminescence intensity tends to decline as the baking temperature rises, indicating that the thermal degradation occurs when the phosphor powder is exposure to air at high temperature. The luminescence is degraded by ~ 10% when the baking temperature is below 500°C, but reduced suddenly by 30% at 600°C. It means that the phosphor surface changes greatly when the sample is baked at 600°C. Compared to a commercially available $SrSi_2O_2N_2:Eu$ phosphor, the phosphor prepared in this work shows much smaller thermal degradation. For example, the efficiency of the commercial one degrades by 40 and 55% at 500 and 600°C, respectively. This great difference is attributable to the following facts: (i) the commercial one contains some amounts of impurity orthosilicate phases that have lower thermal

stability; and (ii) the crystallinity of the commercial phosphor is lower than that of the phosphor prepared in this work (Fig. 6). It clearly implies that both of the phase purity and particle crystallinity (*i.e.*, the surface state) have a great impact on the thermal degradation of a phosphor.
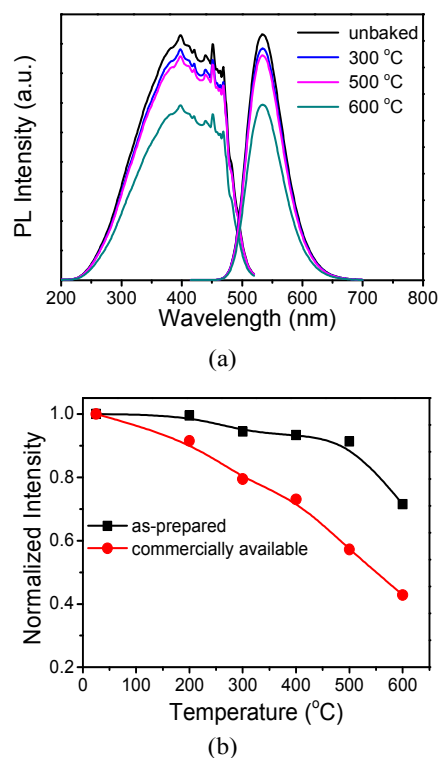

(a)

(b)

Fig. 5 (a) PL excitation and emission spectra of $SrSi_2O_2N_2:0.03Eu^{2+}$ phosphor baked at various temperatures and (b) the normalized intensity as a function of the baking temperature (λ_{ex} = 398nm, λ_{em} = 534nm). For comparison, the data of a commercially available phosphor are included.

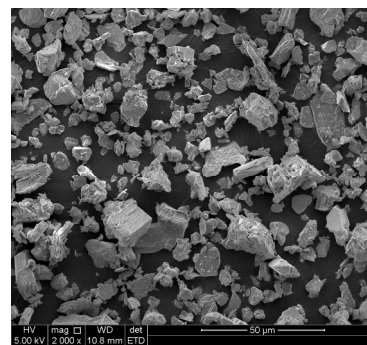**Fig. 6** SEM image of a commercially available $SrSi_2O_2N_2:Eu^{2+}$ phosphor

3.4 TEM observations of the surface states of phosphors

To clarify the thermal degradation mechanism, the surface states of the baked phosphor were analyzed by TEM observations and XPS techniques. As shown in Fig. 7(a), the sample before baking shows well crystallized particles with clean surfaces. On the other hand, there appears some

protuberance on the surface of phosphor particles when baked at 600°C (Fig. 7b). These tiny particles on the phosphor surface are identified to $SrSiO_3$ in both amorphous and crystalline forms. It indicates that the oxidation of $SrSi_2O_2N_2$ happens under high temperature baking, leading to the formation of $SrSiO_3$ attached to the surface of $SrSi_2O_2N_2:Eu^{2+}$ particles. As the orthosilicate phase has rather low thermal stability, it thus accounts for the thermal degradation of $SrSi_2O_2N_2:Eu^{2+}$.
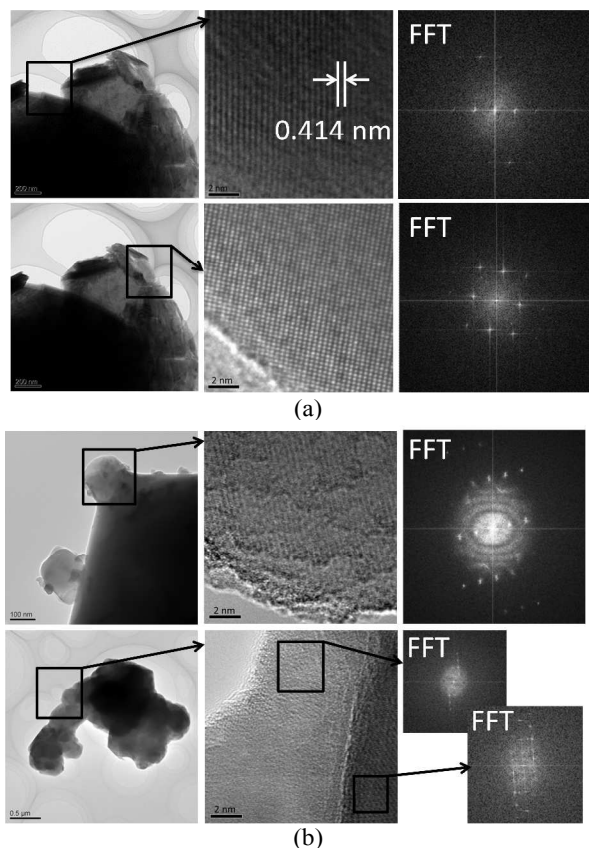

(a)

(b)

Fig. 7 TEM and HRTEM images of phosphor powders without baking (a) and baked at 600 °C (b), respectively (FFT = Fast Fourier Transform).

3.5 X-ray photoelectron spectroscopy (XPS)

The surface states of phosphors were also investigated by XPS. Fig. 8 presents high resolution XPS spectra of O 1s, N 1s, Si 2p, Eu 4d for phosphors before and after baking at 600°C for 2 h. The O1s core-level XPS spectrum displays an asymmetric shape, which can be deconvoluted into two main peaks and one side peak. The binding energy of O 1s in H_2O, SiO_2 and SrO is 533.0, 532.0 and 530.5 eV, respectively.[32-35] Therefore, the highest BE (533.40 eV) is assigned to the O-H bonds, the 532.07 eV is attributed to Si-O bonds, and the lowest BE (530.18 eV) is associated with Sr-O bonds.[32-35] The O 1s XPS spectrum of the baked sample is seen to slightly shift to lower binding energy and to be stronger than that of the unbaked sample. The core-level XPS spectrum of N 1s shows nearly a symmetric shape. The binding energy at 397.17~396.97 eV and

398.91~398.38 eV is ascribed to N 1s the Si-N and Sr-N bonds, respectively.[36,37]

Unlike the O 1s and N 1s core-level XPS spectra, the core-level Si 2p and Eu 4d spectra of the unbaked phosphor are obviously different from those of the baked sample. The Si 2p spectrum of the unbaked sample can be deconvoluted into two peaks located at 101.25 and 102.21 eV, whereas three peaks can be fitted for the spectrum of the baked sample, with an additional peak at 104.56 eV. The binding energy at 102.21 eV is assigned to $SiON_3$ bonds, and the binding energy at 101.25 eV is from the Si-N bond.[38] The highest binding energy at 104.56 eV is associated with Si-O-Sr bonds,[39] which is resulted from $SrSiO_3$ formed on the surface of the baked powder. The core-level Eu 4d spectra of both the unbaked and baked samples can be deconvoluted into three peaks at 133.11~133.23, 134.78~134.95 and 136.41~136.42 eV. The two main peaks of the spectra (133.11~133.23 and 134.78~134.95 eV) is due to the divalent europium ions and the side peak at 136.41~136.42 eV is assigned to the trivalent europium ions.[40,41] As seen, the intensity of Eu^{3+} becomes stronger in the baked phosphor, indicating the oxidation of Eu^{2+} upon high temperature baking.

The oxidation process is expressed by the following equation:[42]

$$2Eu^{2+} + 1/2O_2(g) + V_O \rightarrow 2Eu^{3+} + O_O^{2-}$$
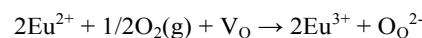
Where V_O is an oxygen vacancy and O_O^{2-} an oxygen ion of the lattice. The oxidation is controlled by the mobility of the Eu^{2+} ion rather than that of oxygen vacancies, and it happens more likely at the phosphor surface.
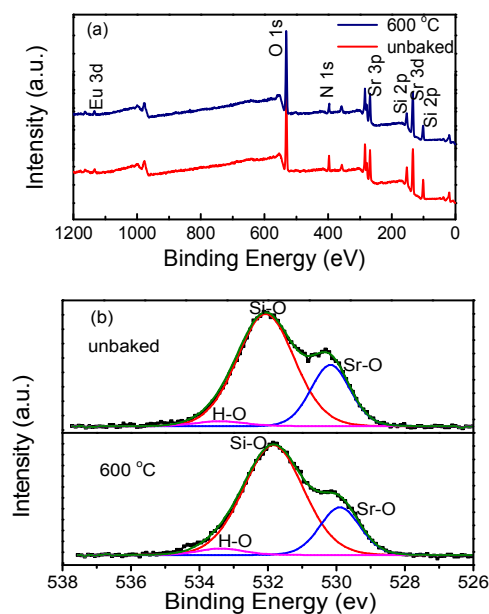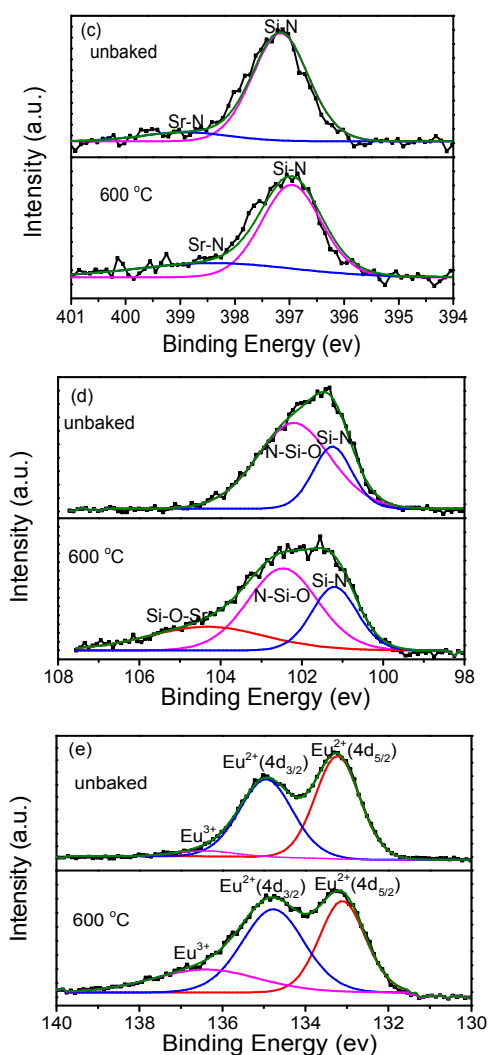
Fig. 8 Wide scan spectra of $SrSi_2O_2N_2:0.03Eu^{2+}$ phosphor as-prepared (a) and XPS spectra of O 1s (b), N 1s (c), Si 2p (d), Eu 4d (e), respectively.

Table2. The corresponding XPS fitting parameters for the samples unbaked and baked at 600°C

Element	unbaked (eV)	Peak intensity (%)	600°C (eV)	Peak intensity (%)
O 1s	533.40	2.75	533.37	3.24
	532.07	70.87	531.84	75.06
	530.18	26.38	529.90	21.71
N 1s	398.91	11.49	398.38	28.74
	397.17	88.51	396.97	71.26
Si 2p	-	-	104.34	24.33
	102.21	71.96	102.47	50.34
	101.25	28.04	101.20	25.33
Eu 4d	136.42	3.49	136.41	20.49
	134.95	45.87	134.78	43.94
	133.23	50.64	133.11	35.57

3.6. TGA and DTA analyses

The thermogravimetric analysis (TGA) and the differential thermal analysis (DTA) curves were recorded by heating the phosphor powders up to 1000°C in air at a heating rate of 5°C/min. As shown in Fig.9, both of the present phosphor and the commercial one firstly undergo a weight loss when heated up to 700°C, and gain weight again when further heated to 1000°C. The weight loss can be ascribed to the release of absorbed water molecule and the residual carbon from the decomposition of the carbonate starting powder. The weight gain is attributable to the oxidation of the phosphor powder when it is exposure to air at high temperature. Compared to the phosphor prepared in this work, the commercial one gains more weight due to oxidation, indicating that the commercial phosphor is more easily oxidized. In addition, an exothermic peak appears at 900°C for both samples, which is due to the oxidation and consistent with the weight gain. Furthermore, the intensity of this exothermic peak is more pronounced for the commercial phosphor, which further evidences its easy oxidation. Therefore, we can come to a conclusion that the thermal stability of the present phosphor is superior to that of the commercial one.
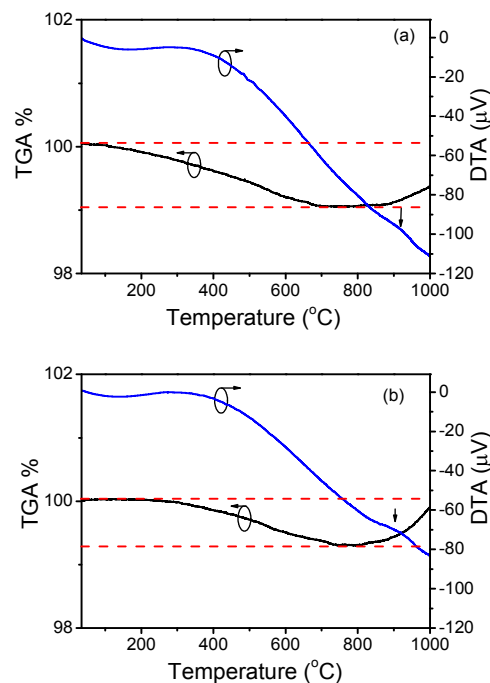

Fig. 9 TGA and DTA curves of $SrSi_2O_2N_2:0.03Eu^{2+}$ phosphor (a) As-prepared and (b) commercially available.

3.7. High temperature in-situ XRD patterns

To elucidate clearly the structural evolution of the phosphor under high temperature baking, the high temperature in-situ X-ray diffraction patterns were measured and shown in Fig. 10. One can see that no impurity phases are identified when the sample is heated to 600°C. Although some amorphous and crystalline $SrSiO_3$ phase can be formed on the phosphor surface at 600°C as discussed before, the total volume of $SrSiO_3$ is too low to be detected by XRD. The $SrSiO_3$ phase, however, is

clearly seen in the sample baked at 1000ºC. It means that the phosphor is seriously oxidized at high temperature.
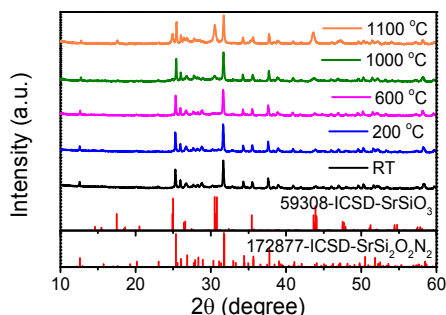

Fig. 10 High temperature in situ XRD pattern of the as-prepared $SrSi_2O_2N_2$:0.03Eu^{2+} phosphor.

3.8 Thermal degradation mechanism

Extensive studies have been done to clarify the mechanism for thermal quenching of LED phosphors, but very few to the thermal degradation mechanism. For the thermal quenching, two dominant models have been proposed to account for the luminescence quenching, i.e., Stokes shift and photoionization. The Stokes shift model is related to the large displacement of the excited state away from the ground state of activators in the configuration coordinate diagram, and the photoionization one to the distance between the bottom of the conduction band and the highest position of the energy levels of the excited activator ions.[5] Differing from thermal quenching, thermal degradation is closely associated with changes in surface states, composition, valence of activators, and etc. In most cases these changes are not irreversible, thus permanently reducing the luminescence efficiency of the phosphor. For example, the thermal degradation of $BaMgAl_{17}O_{19}$:Eu^{2+} (an important blue phosphor for PDPs) during baking is mainly caused by the oxidation of Eu^{2+} to Eu^{3+}.[42,43] As BAM has a layered structure in which Eu^{2+} are sandwiched in between the conduction layers, Eu^{2+} ions are thus easily attacked by oxygen.[44]
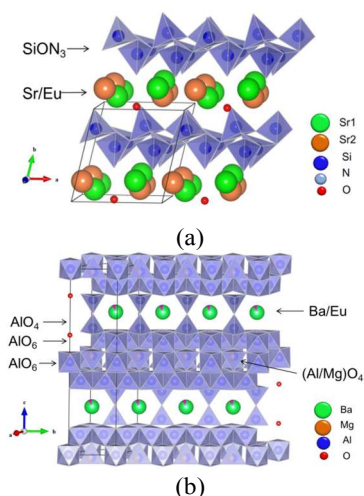

Fig. 11 Crystal structures of (a) $SrSi_2O_2N_2$ and (b) BAM, showing the similar environment around the Eu^{2+} activators.

As to $SrSi_2O_2N_2$, it also has a layered structure in which Eu^{2+} (Sr^{2+}) is located in between the $SiON_3$ layers (Fig.11). Very like BAM:Eu^{2+}, the divalent europium ions in $SrSi_2O_2N_2$ is therefore easily changed to trivalent ones via oxidation, as evidenced in the core-level Eu 4d XPS spectra. This is quite different from the status of Eu^{2+} in α-sialon where it is caged in a polyhedron $[Eu(O,N)_7]$, so that Eu^{2+} is well protected from oxidation.[45,46] Besides the valency change of Eu^{2+}, the oxidation of the host crystal $SrSi_2O_2N_2$ also occurs at high temperature, leading to the formation of $SrSiO_3$, as seen from the TEM images and XRD patterns. Therefore, the thermal degradation of $SrSi_2O_2N_2$:Eu^{2+} can be ascribed to (i) oxidation of activators ($Eu^{2+} \rightarrow Eu^{3+}$), and (ii) oxidation of the host crystal ($SrSi_2O_2N_2 \rightarrow SrSiO_3$). The mechanism is schematically illustrated in Fig. 12.

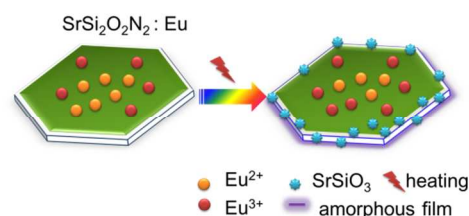**Fig. 12** A schematic showing the thermal degradation mechanism of $SrSi_2O_2N_2$: Eu^{2+}.

As discussed above, thermal degradation lies greatly on the oxidation of phosphors, which is also addressed in $Sr_2Si_5N_8$:Eu^{2+}.[47] In order to minimize the thermal degradation, it is of great importance to protect phosphors from oxidation by surface coatings as reported in BAM:Eu^{2+}. In addition, by comparing the degradation behaviors of two $SrSi_2O_2N_2$:Eu^{2+} investigated in this work, the thermal degradation can also be reduced by improving the crystallinity of phosphor particles, and synthesizing high phase-pure phosphors.

4. Conclusions

In summary, a single phase $SrSi_2O_2N_2$: Eu^{2+} phosphor was obtained by the careful control of the Sr/Si ratio in the starting powder. Compared to a commercial available phosphor, the $SrSi_2O_2N_2$:Eu phosphor prepared in this work showed smaller thermal degradation. With the aid of various analytic techniques, the thermal degradation mechanism was clarified, and was attributed to (i) oxidation of Eu^{2+} to Eu^{3+} and (ii) the formation of the $SrSiO_3$ phase on the phosphor particle surface.

Acknowledgements

Notes and references

a Chinese Academy of Science Key Laboratory of Materials for Energy Conversion, Department of Materials Science and Engineering, University of Science and Technology of China, Hefei, Anhui, People's Republic of China.

b Sialon Group, Sialon Unit, National Institute for Materials Science, Namiki 1-1, Tsukuba, Ibaraki 305-0044, Japan E-mail: Xie.Rong-Jun@nims.go.jp ; Tel: +81 29 860 4312; Fax: +81 29 851 3613

c The Division of Functional Materials and Nanodevices, Ningbo Institute of Materials Technology and Engineering, Chinese Academy of Sciences, Ningbo, Zhejiang 315201,China.

d Department of Materials Science and Engineering, Xiamen University, Xiamen 361005, China.

1   R. -J. Xie, Y. Q. Li, N. Hirosaki and H. Yamamoto, *Nitride Phosphors and Solid-State Lighting*, CRC Press, Boca Raton，2010.

2   R. -J. Xie and N. Hirosaki, *Sci. Tech. Adv. Mater.*, 2007, **8**, 588.

3   J. K. Park, Kim, C. H. Kim, S. H. Park and H. D. Park, *Appl. Phys. Lett.*, 2004, **84**, 1647.

4   P. F. Smet, A. B.Parmentier and D Poelman, *J. Electrochem. Soc.*, 2011, **158**, 37.

5   R. -J. Xie, N. Hirosaki, T. Takeda and T. Suehiro, *ECS J. Solid State Sci. Tech.*, 2013, **2**, R3031.

6   D. Poelman, J. E. Van Haecke and P. F. Smet, *J. Mater. Sci.: Mater. Electron.*, 2009, **20**, 134.

7   R. Yu, J. Wang, M. Zhang, H. Yuan, W. Ding, Y. An and Q. Su, *J. Electrochem. Soc.*, 2008, **155**, J290.

8   G. Z. Cao and R. Metselaar, *Chem. Mater.*, 1991, **3**, 242.

9   S. Yamada, H. Emoto, M. Ibukiyama and N. Hirosaki, *J. Eur. Ceram. Soc.*, 2012, **32**, 1355.

10   C. C. Yang, C. M. Lin, Y. J. Chen, Y. T. Wu, S. R. Chuang, R. S. Liu and S. F. Hu, *Appl. Phys. Lett.*, 2007, **90**, 123503.

11   V. Bachmann, C. Ronda, O. Oeckler, W. Schnick and A. Meijerink, *Chem. Mater.*, 2009, **21**, 316.

12   O. Oeckler, F. Stadler, T. Rosenthal and W. Schnick, *Solid State Sci.*, 2007, **9**, 205.

13   R. -J. Xie, N. Hirosaki, H. L. Li, Y. Q. Li and M. Mitomo, *J. Electrochem. Soc.*, 2007, **154**, J314.

14   Y. C. Fang, P. C. Kao, Y. C. Yang, and S. Y. Chu, *J. Electrochem. Soc.*, 2011, **158**, J246.

15   Y. Q. Li, A. C. A. Delsing, G. de With and H. T. Hintzen, *Chem. Mater.*, 2005, **17**, 3242.

16   B. G. Yun, K. Machida and H. Yamamoto, *J. Ceram. Soc. Jpn.*, 2007, **115**, 619.

17   C. W. Yeh, Y. Li, J.Wang and R. S. Liu, *Opt. Express*, 2012, **20**, 18031.

18   R. S. Liu, Y. H. Liu, N. C. Bagkar, and S. F. Hu, *Appl. Phys. Lett.*, 2007,**91**, 061119.

19   X. F. Song, R. L. Fu, S. Agathopoulos, H. He, X. R. Zhao and R. Li, *J. Electrochem. Soc.*, 2010, **157**, J34.

20   S. D. Jee, K. S. Choi and J. S. Kim, *Met. Mater. Int.*, 2011, **17**, 655.

21   V. Bachmann, T. Justel, A. Meijerink, C. Ronda and P. J. Schmidt, *J. Lumin.*, 2006, **121**, 441.

22   J. Botterman, K. Van den Eeckhout, A. J. J. Bos, P. Dorenbos and P. F. Smet, *Opt. Mater. Express*, 2012, **2**, 341.

23   J. Ruan, R. -J. Xie, N. Hirosaki and T. Takeda, *J. Electrochem. Soc.*, 2012, **159**, H66.

24   X. F. Song, H. He, R. L. Fu, D. L. Wang, X. R. Zhao and Z. W. Pan, *J. Phys. D: Appl. Phys.*, 2009, **42**, 065409.

25   D. W. Suh, G. Anoop, I. H. Cho, J. S. Yoo, S. Y. Kim and S. H. Shin, *J. Ceram. Process. Res.*, 2013, 14, 139.

26   K. Y. Jung and J. H. Seo, *Electrochem. Solid-State Lett.*, 2008,**11**, J64.

27   X. F. Yang, H. L. Song, L. X. Yang, and X. Xu, *J. Am. Ceram. Soc.*,2011, **94**, 28.

28   B. Y. Han and K. S. Sohn, *Electrochem. Solid-State Lett.*,2010, **13**, J62.

29   J. Y. Tang, X. F. Yang, C. Zhan, L. Y. Hao, X. Xu and W. H. Zhang, *J. Mater. Chem.*, 2012, **22**, 488.

30   B.-G. Yun, Y. Miyamoto and H. Yamamoto, *J. Electrochem. Soc.*2007, **154**, J320.

31   W. H. Zhu, P. L. Wang, W. Y. Sun and D. S. Yan, *J. Mater. Sci. Lett.*, 1994, **13**, 560.

32   J. F. Moulder, W. F. Stickle, P. E. Soble and K. D. Bomben, *Handbook of X-ray Photoelectron Spectroscopy,* Physical Electronics Inc., U.S.A.,1992.

33   B. Marchon, J. Carrazza, H. Heinemann and G. A. Somorjai, *Carbon,* 1988, **26**, 507.

34   H. J. Martin, K. H. Schulz, J. D. Bumgardner and K. B. Walters, *Appl. Surf. Sci.*, 2008, **254**, 4599.

35   R.P. Vasquez, *J. Electron. Spectrosc. Relat. Phenom.*,1991, **56**, 217.

36   I. Bertoti, G. Varsányi, G. Mink T. Szekely, J. Vaivads, T. Millers and J. Grabis, *Surf. Interface Anal.*, 1988, **12**, 527.

37   P. D. Kirsch and J. D. Ekerdt, *J. Vac. Sci. Technol., A*, 2001, **19**, 2222.

38   V. A. Gritsenko, R.W. M. Kwok, H. Wong and J. B. Xu, *J. Non-Cryst. Solids*, 2002, **297**, 96.

39   X. F. Xu, X. J. Niu, J. Fan, Y. N. Wang and M. Feng, *J. Nat. Gas Chem.*, 2011, **20,** 543.

40   W. D. Schneider, C. Laubschat, I. Nowik and G. Kaindl, *Phys. Rev. B*, 1981, **24**, 5422.

41   J. Qi, T. Matsumoto, M. Tanaka and Y. Masumoto, *J. Phys. D: Appl. Phys.*, 2000, **33**, 2074.

42   G. Bizarri and B. Moine, *J. Lumin.*, 2005, **113**, 199.

43   K. B. Kim, K. W. Koo, T. Y. Cho and H. G. Chun, *Mater. Chem. Phys.*, 2003, **80**, 682.

44   Y. I. Kim, S. O. Kang, J. S. Lee, M. J. Jung and K. H. Kim, *J. Mater. Sci. Lett.*, 2002, **21**, 219.

45   R. -J. Xie, N. Hirosaki, K. Sakuma, Y. Yamamoto and M. Mitomo, *Appl. Phys. Lett.*, 2004, **84**, 5404.

46   R. -J. Xie, M. Mitomo, K. Uheda, F. F. Xu and Y. Akimune, *J. Am. Ceram. Soc.*, 2002, **85**, 1229.

47   C. W. Yeh, W. T. Chen, R. S. Liu, S. F. Hu, H. S. Sheu, J. M. Chen and H. T. Hintzen, *J. Am. Chem. Soc.*, 2013, **134**, 14108.